SANDIA REPORT

SAND2004-4770
Unlimited Release
Printed September 2004

Autofocus Correction of Excessive Migration in Synthetic Aperture Radar Images

Armin W. Doerry

Prepared by
Sandia National Laboratories
Albuquerque, New Mexico 87185 and Livermore, California 94550

Sandia is a multiprogram laboratory operated by Sandia Corporation, a Lockheed Martin Company, for the United States Department of Energy under Contract DE-AC04-94AL85000.

Approved for public release; further dissemination unlimited.

Issued by Sandia National Laboratories, operated for the United States Department of Energy by Sandia Corporation.

NOTICE: This report was prepared as an account of work sponsored by an agency of the United States Government. Neither the United States Government, nor any agency thereof, nor any of their employees, nor any of their contractors, subcontractors, or their employees, make any warranty, express or implied, or assume any legal liability or responsibility for the accuracy, completeness, or usefulness of any information, apparatus, product, or process disclosed, or represent that its use would not infringe privately owned rights. Reference herein to any specific commercial product, process, or service by trade name, trademark, manufacturer, or otherwise, does not necessarily constitute or imply its endorsement, recommendation, or favoring by the United States Government, any agency thereof, or any of their contractors or subcontractors. The views and opinions expressed herein do not necessarily state or reflect those of the United States Government, any agency thereof, or any of their contractors.

Printed in the United States of America. This report has been reproduced directly from the best available copy.

Available to DOE and DOE contractors from

U.S. Department of Energy
Office of Scientific and Technical Information
P.O. Box 62
Oak Ridge, TN 37831

Telephone: (865)576-8401
Facsimile: (865)576-5728
E-Mail: reports@adonis.osti.gov
Online ordering: http://www.doe.gov/bridge

Available to the public from

U.S. Department of Commerce
National Technical Information Service
5285 Port Royal Rd
Springfield, VA 22161

Telephone: (800)553-6847
Facsimile: (703)605-6900
E-Mail: orders@ntis.fedworld.gov

Online order: http://www.ntis.gov/ordering.htm

SAND2004-4770
Unlimited Release
Printed September 2004

Autofocus Correction of Excessive Migration in Synthetic Aperture Radar Images

Armin W. Doerry
Synthetic Aperture Radar Department

Sandia National Laboratories
PO Box 5800
Albuquerque, NM 87185-0519

ABSTRACT

When residual range migration due to either real or apparent motion errors exceeds the range resolution, conventional autofocus algorithms fail. A new migration-correction autofocus algorithm has been developed that estimates the migration and applies phase and frequency corrections to properly focus the image.

ACKNOWLEDGEMENTS

Some of the concepts described herein originated in discussions with Freddie Heard regarding anomalies observed in Sandia developed fielded systems. Aspects of several concepts described herein were also used for data analysis by Freddie Heard and Tom Cordaro, and perhaps others.

This work was funded by the US DOE Office of Nonproliferation & National Security (NNSA), Office of Research and Development, Proliferation Detection Program Office (NA-22), under the Advanced Radar System (ARS) project.

CONTENTS

FOREWORD

Sandia developed high-performance Synthetic Aperture Radar (SAR) systems push the envelope of feasibility on a number of fronts, including fine resolution at long ranges. Several years ago, fielded systems began occasionally exhibiting image quality problems that were traced to apparent excessive residual migration. Low-frequency, long-aperture Sandia test systems such as the Concealed Target SAR (CTSAR) exhibited the same anomalies. Then future systems such as the Ka-band Ultra-High-Resolution SAR (UHRSAR) were expected to do the same, and did. Even the Ku-band MiniSAR currently under development is expected to encounter excessive residual migration depending on which inertial motion measurement sensor instruments are used. Finally, the literature began reporting that even with perfect motion measurement, atmospheric anomalies would cause an apparent excessive migration in the data.

After determining the limitations of existing autofocus algorithms, new techniques were explored and developed to accommodate excessive residual migration. These have proved effective in ground processing of images from fielded systems, CTSAR, and UHRSAR. This report details these techniques.

1. Introduction & Background

Synthetic Aperture Radar (SAR) forms images of a scene by sampling energy from a scattered field along the radar's flight path and coherently processing the data. Coherence of the data set is facilitated by very accurately measuring the geometric relationship between the desired target scene and the radar's flight path, and accounting for this in the data processing. This requires measuring the radar's motion, or at least its relative motion, very accurately and with fractional-wavelength precision over the course of the synthetic aperture. Typically, an Inertial Measurement instrument is employed, and even this is often aided by Global Positioning Satellite navigation readings.

The raw SAR data is typically a two-dimensional array of complex data samples, with one dimension representing samples from echoes of individual pulses (fast-time), and the other dimension representing the pulse index number (slow-time). This collection is termed the phase history data. Since wideband modulation techniques, such as the Linear Frequency Modulated (LFM) chirp waveform, are normally used for individual pulses, the data needs to be processed, or compressed, in the intra-pulse or range direction to achieve the final desired range resolution. This is termed range-compression. The data needs further processing in the inter-pulse or azimuth direction to complete the image formation process. This is termed azimuth compression.

During the course of a synthetic aperture, as the radar's perspective towards a target scene changes, ranges to some target locations change or migrate relative to other target locations. This migration is deterministic and is compensated within the image formation process by algorithms such as the Polar Format Algorithm (PFA) developed by Walker.[1]

Relatively small motion measurement errors manifest themselves principally as phase errors in the complex data samples, and if large enough become observable as a smearing, blurring, or other degradation in the image. For most SAR systems, however, the nature and degree of blurring is nearly identical in different parts of the degraded SAR image. This allows a measurement of the blurring function, and then a calculation of a suitable correction to be applied to the original data to compensate for the presumed motion error. Further processing then may yield a well-focused image devoid of the previously observable degradation. A number of algorithms exist to automatically focus the degraded image. While some measure and compensate blurring, others seek to optimize other measures, such as contrast ratio in the image. Collectively, these processes are termed "autofocus" algorithms. A very popular autofocus algorithm is the Phase Gradient Autofocus (PGA) algorithm described by Wahl, et. al.[2]

Very large relative motion measurement errors manifest themselves as an unexpected additional shifting or migration of target locations beyond the aforementioned deterministic migration during the course of the synthetic aperture. Degradation in images from data exhibiting errors of this magnitude are substantial, often rendering the image useless. Application of conventional autofocus techniques are unable to properly mitigate the image degradation. It is this problem that this report addresses.

Figure 1 is a photograph of a SAR imaging test site used to evaluate image quality. Figure 2 is a SAR image of the same scene created using PFA processing but without any autofocus applied. The data set was collected at a 41 km range and offers a capability of 4-inch resolution, but this image exhibits severe smearing in the azimuth direction. Figure 3 is a rendering of the range-compressed data, but with deterministic migration compensated. Figure 4 details a single trihedral target reflector's track in the range-compressed data. The departure of this track from a straight horizontal line illustrates problematic excessive uncompensated residual migration. Figure 5 illustrates how a conventional autofocus algorithm (PGA in this case) is unable to properly correct for this, and causes the "double-vision" effect.

A general presumption in the SAR community is that any motion measurement errors are less than the range resolution of the radar. This infers that the track in Figure 4 is contained within a single row of resolution cells (which it is not). This further allows the conventional practice of autofocus operations being adequately applied to fully range-compressed images. Since autofocus typically requires iteratively processing the data into an image, efficiency is gained by repeating only the azimuth compression, and not the range compression operations. This presupposes that, for example, a radar with 2 cm nominal wavelength and 30 cm range resolution will never see more than $(4\pi/\lambda)\rho_r = 60\pi$ radians of phase error.

Figure 1. Photograph of SAR test and evaluation site.

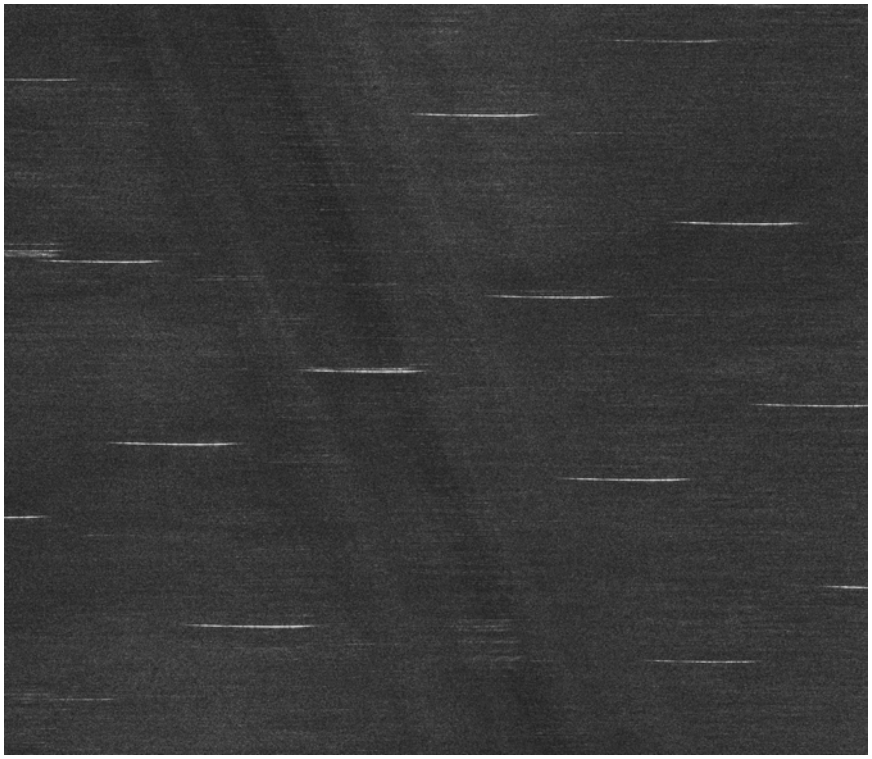

Figure 2. SAR image of test site using PFA processing but no autofocus.

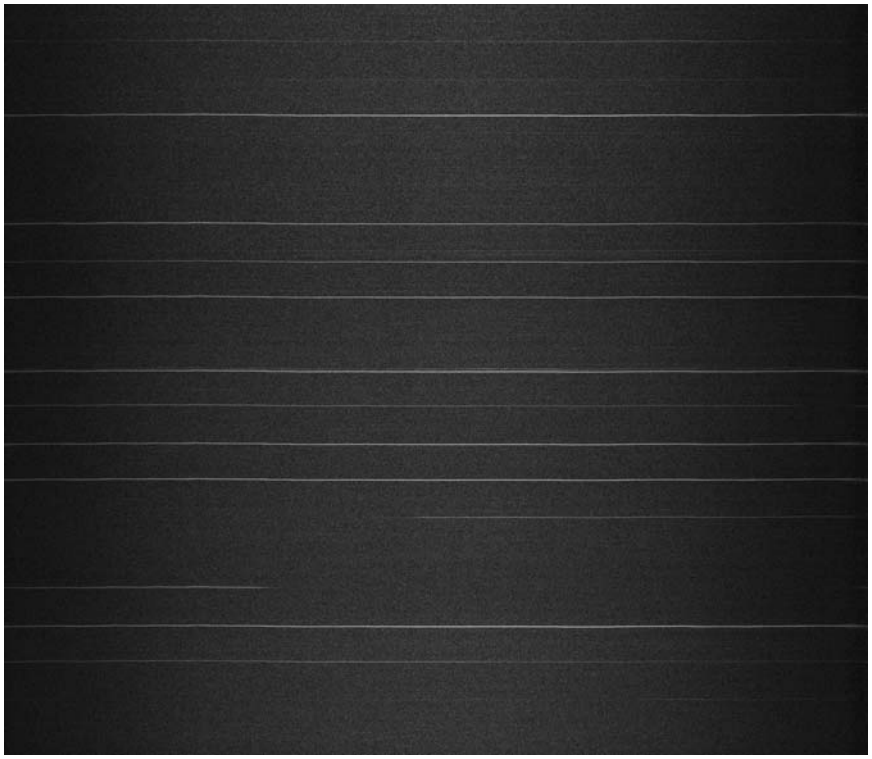

Figure 3. Range-compressed data with deterministic migration corrected.

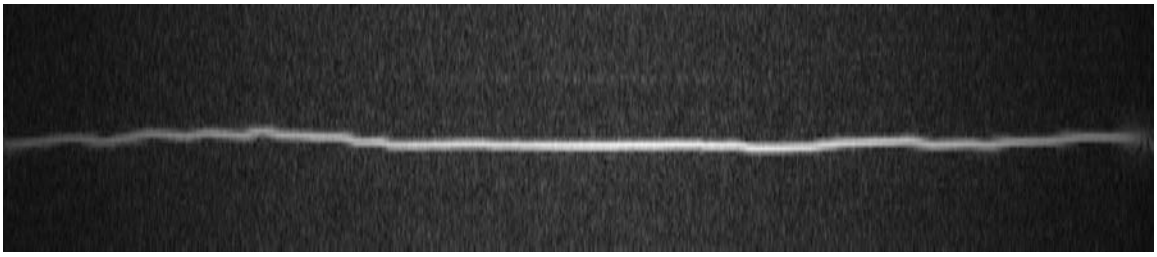

Figure 4. Detail of trihedral target reflector track in range-compressed data.

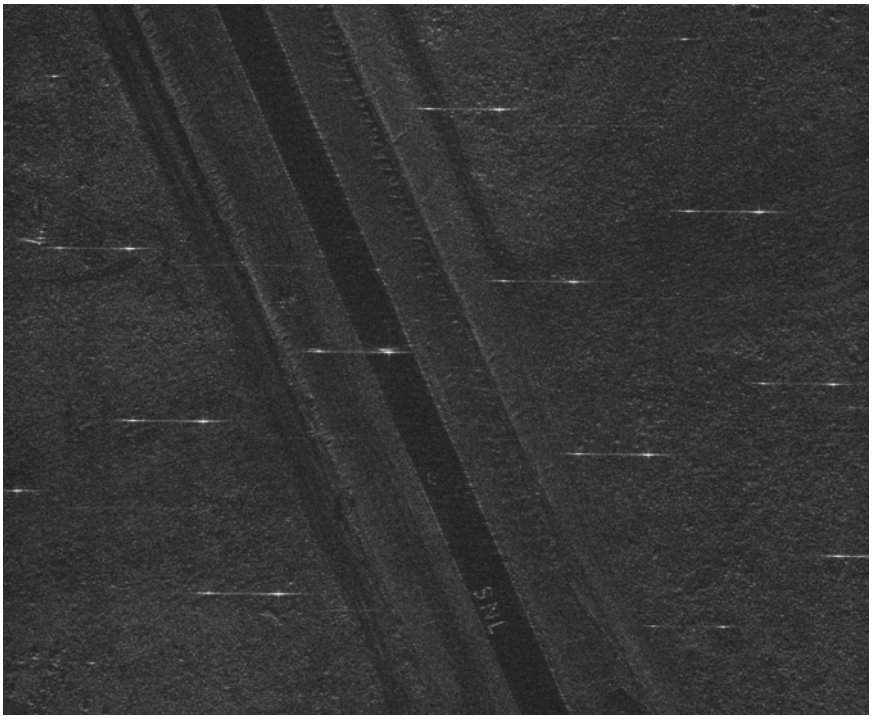

Figure 5. Conventional PGA autofocus applied to image of Figure 2.

Jakowatz, et. al,[3] state that "maintaining relative-position uncertainties of the SAR platform to well less than a range-resolution cell size (e.g., 1 meter) is easily achievable by modern inertial navigation systems." Furthermore, "[i]n practice the size of the [range error] shift, $\varepsilon c/2$, is a small fraction of the resolution cell size."

Carrara, et. al,[4] describe several different autofocus techniques, with all but one operating on range-compressed data. The exception is a technique called Prominent Point Processing, which they describe being "considered a refocus technique, although it is not technically *automatic*." This technique depends on selecting scatterers in the image that are point-like, otherwise risking "serious degradation if the scatterer selected as the prominent point is not a point scatterer but rather a more complex target within a range resolution cell." Furthermore, "Selection of the prominent point is typically an interactive process requiring user inputs; however, the state of the art is progressing toward automation of this process." Nevertheless, no autofocus techniques are described

or discussed that mitigate excessive residual migration in general SAR images, especially those without clear and distinct point-like target features.

In addition to motion measurement errors, longer ranges impart greater deleterious atmospheric effects to the data, whereby electrical path lengths depart significantly from the physical path lengths. The electrical path length is related to the actual path length by the ratio of the average wavelength to the nominal wavelength, and accounts for atmospheric dielectric variations, refraction and other wave propagation phenomena. Since coherence depends on electrical path lengths, problematic errors similar to motion measurement errors may be induced by perturbations in the atmosphere's transmission characteristics in spite of perhaps otherwise adequate motion measurements.

Denny & Scott[5] claim that "the performance of future high-resolution SAR modes will be limited by anomalous propagation effects, rather than by platform measurement errors or focusing algorithm limitations, or RF wavelength." Their conclusion is based on the assumption that uncompensated apparent (due to anomalous propagation) range variations equal to the range resolution is "the rule-of-thumb limit that can be achieved, using autofocus."

While the presumption of apparent range errors being less than the radar's range resolution is often true, modern high-performance SARs do sometimes exceed this criterion. The drive for finer resolutions, longer ranges, and less expensive (and less accurate) motion measurement systems will increasingly cause situations where a target's echo return effectively exhibits a residual migration error exceeding one or more range resolution cells during the course of the synthetic aperture. This would doom to failure any autofocus scheme that presupposes otherwise, which includes autofocus schemes that operate only on fully range-compressed data.

While most autofocus algorithms apply a phase-correction to range-compressed data, the more accurate remedy is to apply a range-shift to the range-compressed data.

Burns & Cordaro[6] correct deterministic range migration during the course of image formation by a shifting operation that is implemented via multiplying the uncompressed range vectors with a parameter dependent specific sinusoid. However residual migration due to motion measurement errors is not addressed.

Carrera, et. al,[4] do use a track of a prominent point's peak location in the range compressed image to "adjust the frequency of each pulse in the original signal history." As previously stated, however, determining the amount of adjustment for their technique depends on tracking a prominent point-like scatterer, thereby limiting its utility to SAR images with this characteristic.

2. Overview & Summary

Two tasks are at hand.

The initial task is to properly measure the residual migration and phase error. This may be accomplished by either of two methods.

The first measurement method recognizes that a phase error function in the azimuth direction cannot be ascertained from a fully range-compressed data set, since the error energy is spread across several range resolution widths. Therefore it must occur under the constraint that for extracting the autofocus correction vector, the range resolution must be coarse enough to encompass the phase error. Put another way, the phase error must be measured on data that is not fully range compressed, i.e. radar data with degraded range resolution. This can be done by using only part of each return echo, that is, a portion of the fast-time vector. It can also be done by blurring the fully range-compressed data in the range dimension. If range subapertures are used for image formation, then perhaps a single range subaperture might be employed for phase-error measurement. Once an accurate phase error has been measured then the corresponding migration effects can be calculated.

An alternate, or second measurement method determines the actual migration effects by correlating range-compressed pulses with each other. This process of correlating range profiles obviates the need for identifying and selecting a prominent scatterer, allowing improved performance on SAR images not containing prominent points.

The final task begins once the migration effects have been adequately characterized. A compensation must then be properly applied to the SAR data. The excessive range migration must be mitigated, that is, excessive range shifts in range-compressed data must be eliminated. The echo returns must be shifted back into proper position. Range shifts in range-compressed data are achieved by multiplying the uncompressed data with a fast-time-dependent phase shift, that is, a complex sinusoid that shifts frequency in addition to phase in the manner of the Prominent Point Processing method. Consequently, the data correction operation must occur prior to full range compression. Optimally, it is applied to the phase-history data prior to any range compression at all, but might also be done in only partially range-compressed data when range subapertures are employed.

3. Detailed Analysis

We begin the analysis by assuming the target as an isotropic point scatterer, and the waveform is a Linear Frequency Modulated (LFM) chirp. The radar echo from a point target may be adequately described in the phase history data by

$$X_V(t,n) \approx$$
$$A_s \operatorname{rect}\left(\frac{t - t_n - \frac{2}{c}\left|\mathbf{r}_{s,n}\right|}{T} \right) \exp j\left\{ \frac{2\omega_n}{c}\left[1 + \frac{\gamma_n}{\omega_n}\left(t - t_n - \frac{2}{c}\left|\mathbf{r}_{c,n}\right| \right) \right] \left(\left|\mathbf{r}_{c,n}\right| - \left|\mathbf{r}_{s,n}\right| \right) \right\} \tag{1}$$

where

A_s = the target response amplitude,
T = pulse width of the radar,
n = the slow-time pulse index number with $N/2 \le n < N/2$,
ω_n = the center frequency of the nth pulse,
γ_n = the chirp rate of the nth pulse,
t_n = time of the nth pulse,
t = time,
c = the velocity of propagation,
$\mathbf{r}_{c,n}$ = vector from the target scene focal point to the radar for the nth pulse, and
$\mathbf{r}_{s,n}$ = vector from the specific point target to the radar for the nth pulse.

The radar's motion measurement system measures $\mathbf{r}_{c,n}$. If the measurement is in error by some vector $\boldsymbol{\varepsilon}_n$ for the nth pulse, then the echo data will be of the form

$$X_V(t,n) \approx$$
$$A_s \operatorname{rect}\left(\frac{t - t_n - \frac{2}{c}\left|\mathbf{r}_{s,n}\right|}{T} \right) \exp j\left\{ \frac{2\omega_n}{c}\left[1 + \frac{\gamma_n}{\omega_n}\left(t - t_n - \frac{2}{c}\left|\mathbf{r}_{c,n} + \boldsymbol{\varepsilon}_n\right| \right) \right] \left(\left|\mathbf{r}_{c,n} + \boldsymbol{\varepsilon}_n\right| - \left|\mathbf{r}_{s,n}\right| \right) \right\}. \tag{2}$$

Particularly problematic is the line-of-sight component of the motion measurement error, that we denote

$$\varepsilon_n = \frac{\boldsymbol{\varepsilon}_n \bullet \mathbf{r}_{c,n}}{\left|\mathbf{r}_{c,n}\right|}. \tag{3}$$

Other error components have minor impact on SAR image quality by comparison. This allows the approximation

$$X_V(t,n) \approx \tag{4}$$
$$A_s \operatorname{rect}\left(\frac{t - t_n - \frac{2}{c}\left|\mathbf{r}_{s,n}\right|}{T} \right) \exp j\left\{ \frac{2\omega_n}{c}\left[1 + \frac{\gamma_n}{\omega_n}\left(t - t_n - \frac{2}{c}\left|\mathbf{r}_{c,n}\right| - \frac{2}{c}\varepsilon_n \right) \right] \left(\left|\mathbf{r}_{c,n}\right| - \left|\mathbf{r}_{s,n}\right| + \varepsilon_n \right) \right\}.$$

After sampling, the digital data set is described by

$$X_V(i,n) \approx A_s \exp j\left\{ \frac{2\omega_n}{c}\left[1 - \left(\frac{2\gamma_n}{\omega_n c} \right)\varepsilon_n + \frac{\gamma_n}{\omega_n} T_{s,n} i \right] \left(\left|\mathbf{r}_{c,n}\right| - \left|\mathbf{r}_{s,n}\right| + \varepsilon_n \right) \right\} \tag{5}$$

where

$T_{s,n}$ = the fast-time sampling rate for the nth pulse, and
i = the fast-time sample index number with $I/2 \le i < I/2$.

By making the usual assumption of a flat image plane, we identify

$$\left|\mathbf{r}_{c,n}\right| - \left|\mathbf{r}_{s,n}\right| \approx \cos\psi_n \cos\alpha_n \left(s_x \tan\alpha_n - \frac{s_r}{\cos\psi_0} \right) \tag{6}$$

where

s_x = target offset from scene focal point in the azimuth direction,
s_r = target offset from scene focal point in the slant-range direction,
ψ_n = actual pulse-to-pulse grazing angle for $\mathbf{r}_{c,n}$, and
ψ_0 = single nominal grazing angle for all $\mathbf{r}_{c,n}$, and
α_n = azimuthal angle for $\mathbf{r}_{c,n}$, with respect to the center of the synthetic aperture.

By further noting that the first occurrence of ε_n is of negligible practical consequence, the digital data can then be expanded to

$$X_V(i,n) \approx \tag{7}$$
$$A_s \exp j\left\{ \frac{2\omega_n}{c}\left[1 + \frac{\gamma_n}{\omega_n}\left(T_{s,n} i \right) \right] \cos\psi_n \cos\alpha_n \left(s_x \tan\alpha_n - \frac{s_r - \left(\frac{\cos\psi_0}{\cos\psi_n \cos\alpha_n} \right)\varepsilon_n}{\cos\psi_0} \right) \right\}.$$

Deterministic migration is compensated by sampling/resampling the data onto a rectangular grid prior to application of efficient Fast Fourier Transform techniques. This may be accomplished by familiar methods and effects

$$\left(\gamma_n T_{s,n} \cos\psi_n \cos\alpha_n\right) i = \left(\gamma_0 T_{s,0} \cos\psi_0\right) i' \text{, and} \tag{8}$$

$$\left(\omega_n \cos\psi_n \cos\alpha_n + \left(\gamma_0 T_{s,0} \cos\psi_0\right) i'\right) \tan\alpha_n = \left(\omega_0 \cos\psi_0 d\alpha\right) n' \tag{9}$$

where

$d\alpha$ = a nominal azimuth sampling frequency scale factor,
ω_0 = the nominal center frequency,
γ_0 = the nominal chirp rate,
$T_{s,0}$ = the nominal fast-time sampling rate,
i' = the new fast-time sampling index with $I'/2 \le i' < I'/2$,
n' = the new slow-time sampling index with $N'/2 \le n' < N'/2$.

While this corrects for deterministic migration, it also impacts the nature of ε_n in the 'corrected' data. By defining ε_n as specifically a function of α_n we can calculate its dependence on the new indices as

$$\varepsilon_n = \varepsilon(\alpha_n) = \varepsilon\left(\text{atan}\left(\frac{d\alpha\, n'}{\left(\frac{\omega_n}{\omega_0}\right)\left(\frac{\cos\psi_n \cos\alpha_n}{\cos\psi_0}\right) + \left(\frac{\gamma_0 T_{s,0}}{\omega_0}\right) i'} \right) \right). \tag{10}$$

For typical resolutions where the range of α_n is small, this approximates to

$$\varepsilon_n \approx \varepsilon\left(\frac{d\alpha\, n'}{\left(\frac{\omega_n}{\omega_0}\right)\left(\frac{\cos\psi_n \cos\alpha_n}{\cos\psi_0}\right) + \left(\frac{\gamma_0 T_{s,0}}{\omega_0}\right) i'} \right). \tag{11}$$

A byproduct of the sampling/resampling is typically that $\omega_n = \omega_0 \cos\psi_0 / \cos\psi_n \cos\alpha_n$. The error then becomes

$$\varepsilon_n \approx \varepsilon\left(\frac{d\alpha\, n'}{1 + \left(\frac{\gamma_0 T_{s,0}}{\omega_0}\right) i'} \right). \tag{12}$$

Data corrected for deterministic migration to facilitate image formation using for example the Polar Format Algorithm yields

$$X_V(i',n') \approx A_s \exp j\left\{\frac{2\omega_0}{c}\cos\psi_0 s_x d\alpha\ n' - \frac{2\gamma_0 T_{s,0}}{c}\left(s_r - \varepsilon'_{n',i'}\right)i' - \frac{2\omega_0}{c}\left(s_r - \varepsilon'_{n',i'}\right)\right\} \quad (13)$$

where the error term has been slightly modified and become

$$\varepsilon'_{n',i'} = \left(\frac{\cos\psi_0}{\cos\psi_n \cos\alpha_n}\right)\varepsilon_n . \quad (14)$$

As a practical matter, it is often adequate to assume

$$\varepsilon'_{n',i'} \approx \varepsilon_n . \quad (15)$$

By recognizing that the achievable nominal resolutions of this data set are

$$\rho_r = \frac{2\pi c}{2\gamma_0 T_{s,0} I'} = \text{slant range resolution, and} \quad (16)$$

$$\rho_a = \frac{2\pi c}{2\omega_0 N' d\alpha \cos\psi_0} = \text{azimuth resolution,} \quad (17)$$

and ignoring a constant phase term, the data model may be rewritten as

$$X_V(i',n') \approx A_s \exp j\left\{\frac{2\pi}{N'}\left(\frac{s_x}{\rho_a}\right)n' - \frac{2\pi}{I'}\left(\frac{s_r - \varepsilon'_{n',i'}}{\rho_r}\right)i' + \frac{4\pi}{\lambda_0}\varepsilon'_{n',i'}\right\} \quad (18)$$

where the nominal wavelength $\lambda_0 = 2\pi c/\omega_0$.

A first order expansion of $\varepsilon'_{n',i'}$ yields approximately

$$\varepsilon'_{n',i'} \approx \varepsilon'_{n',0} + \left(\frac{d\varepsilon'_{n',i'}}{di'}\right)i' \approx \varepsilon(d\alpha\ n'\ ) + \left(\frac{d\varepsilon(\alpha_n)}{d\alpha_n}\right)\left(\frac{d\alpha_n}{di'}\right)i' \quad (19)$$

or approximately

$$\varepsilon'_{n',i'} \approx \varepsilon(d\alpha\ n'\ ) - \left(\frac{d\varepsilon(\alpha_n)}{d\alpha_n}\right)\left(\frac{\gamma_0 T_{s,0}}{\omega_0}\right)(d\alpha\ n')\,i' . \quad (20)$$

This allows the data model to be rewritten as

$$X_V(i',n') \approx$$

$$A_s \exp j\left\{ \frac{2\pi}{N'}\left(\frac{s_x}{\rho_a}\right) n' + \frac{2\pi}{I'}\left(\frac{\varepsilon(d\alpha\, n') - \left(\frac{d\varepsilon(\alpha_n)}{d\alpha_n}\right) d\alpha\, n' - s_r}{\rho_r} \right) i' + \frac{4\pi}{\lambda_0}\varepsilon(d\alpha\, n') \right\}. \quad (21)$$

Recall that the Discrete Fourier Transform (DFT) of a finite-length complex exponential is given by

$$\exp j\{\Omega i'\} \Leftrightarrow \operatorname{csinc}_{I'}\left(\frac{I'}{2\pi}\left(\Omega - \frac{2\pi}{I'}v\right)\right) \quad (22)$$

where

v = the frequency index, and

$$\operatorname{csinc}_{I'}(x) = \frac{\sin(\pi x)}{\sin(\pi x/I')} \exp j\{-\pi x/I'\}.$$

Note that for small (x/I') this approaches

$$\operatorname{csinc}_{I'}(x) \xrightarrow[\text{small}(x/I')]{} I' \operatorname{sinc}(x) = \frac{I' \sin(\pi x)}{\pi x} \quad (23)$$

and has peak value at $x = 0$, and effective unit width, that is, the bulk of its energy falling in the domain $-1/2 < x < 1/2$. Energy outside these limits is generally unusable in addition to being undesirable.

Range compression on our data model entails performing a DFT over index i'. This yields

$$X_{RC}(v,n') \approx$$

$$A_s \operatorname{csinc}_{I'}\left(\left(\frac{\varepsilon(d\alpha\, n') - \left(\frac{d\varepsilon(\alpha_n)}{d\alpha_n}\right) d\alpha\, n' - s_r}{\rho_r} \right) - v \right) \exp j\left\{ \frac{2\pi}{N'}\left(\frac{s_x}{\rho_a}\right) n' + \frac{4\pi}{\lambda_0}\varepsilon(d\alpha\, n') \right\}. \quad (24)$$

Although we developed this expression by range-compressing the resampled phase history data, it should also be obvious that the same form for the data can be achieved by beginning with an image and undoing the azimuth compression step. Furthermore, resampled pseudo-phase history data can be generated by undoing the range compression as well.

This expression has a peak response in range at the index value

$$v_{peak} = \left(\frac{\varepsilon(d\alpha\, n') - \left(\frac{d\varepsilon(\alpha_n)}{d\alpha_n} \right) d\alpha\, n' - s_r}{\rho_r} \right) \tag{25}$$

with energy concentrated in a region of unit width around the peak. We note that this strip is a function of n', that is, the peak location v_{peak} depends on (migrates with) n'. For a single index value v to harbor all the energy requires the constraint

$$\left| \varepsilon(d\alpha\, n') - \left(\frac{d\varepsilon(\alpha_n)}{d\alpha_n} \right) d\alpha\, n' \right| \le \rho_r . \tag{26}$$

This is the customary presumption for autofocus algorithms, as it allows the further approximation

$$X_{RC}(v, n') \approx A_s \operatorname{csinc}_{I'}\left(\left(\frac{-s_r}{\rho_r} \right) - v \right) \exp j\left\{ \frac{2\pi}{N'} \left(\frac{s_x}{\rho_a} \right) n' + \frac{4\pi}{\lambda_0} \varepsilon(d\alpha\, n') \right\} \tag{27}$$

where the original motion error manifests itself only as an azimuth phase error in the range-compressed data, and furthermore is confined to a single range bin for any one scatterer.

This report concerns itself with mitigating the effects of ε_n when we violate the customary constraint in equation (26) and allow excessive migration.

The first step is to characterize the error, that is, finding ε_n or equivalent. The second step is to correct the pre-range-compressed data using this information, and then continue image formation. We describe two techniques for finding ε_n and correcting the data.

Technique 1:

The essence of this technique is to measure a phase error, and calculate a corresponding range-shift. Then phase and frequency corrections are applied to the data to correct both.

We begin this technique by noting that if equation (26) is satisfied, then we can find ε_n in any number of proven manners that rely on a scatterer's energy remaining in a single range resolution cell. One technique with wide popularity is the robust aforementioned Phase Gradient Autofocus algorithm.

The essence of this technique for finding ε_n observes that if equation (26) is violated, we can process the data to a new coarser range resolution ρ_r' so that equation (26) is met with the new resolution. Once done, then ε_n can be found from the new range compressed (to the coarser resolution) data using existing techniques such as PGA.

The coarser range-resolution may be accomplished by any of several means. For example, the complex data can be filtered or blurred in the range dimension. Alternatively, a subset (in the fast-time dimension) of the phase history data set can be used that limits resolution to the desired ρ'_r. In any case, it becomes crucial to select a ρ'_r large enough to accommodate any expected ε_n.

Once the motion error ε_n has been estimated, and by extension $\varepsilon'_{n',i'}$ has been estimated, the pre-range-compressed data can be corrected by multiplying the data in the manner

$$X_{V,\text{corrected}}(i',n') \approx X_V(i',n')\left[\exp j\left\{-\frac{2\pi}{I'}\left(\frac{\varepsilon'_{n',i'}}{\rho_r}\right)i' - \frac{4\pi}{\lambda_0}\varepsilon'_{n',i'}\right\}\right] \tag{28}$$

or approximately

$$X_{V,\text{corrected}}(i',n') \approx$$
$$X_V(i',n')\exp j\left\{-\frac{2\pi}{I'}\left(\frac{\varepsilon(d\alpha\, n') - \left(\frac{d\varepsilon(\alpha_n)}{d\alpha_n}\right)d\alpha\, n'}{\rho_r}\right)i' - \frac{4\pi}{\lambda_0}\varepsilon(d\alpha\, n')\right\} \tag{29}$$

which yields the desired error-free model

$$X_{V,\text{corrected}}(i',n') \approx A_s \exp j\left\{\frac{2\pi}{N'}\left(\frac{s_x}{\rho_a}\right)n' - \frac{2\pi}{I'}\left(\frac{s_r}{\rho_r}\right)i'\right\}. \tag{30}$$

Data corrected this way may be processed into an image in the usual manner, for example with a two-dimensional Fourier transform.

Note that the data correction is both a fast-time frequency shift and a phase shift. While typical autofocus algorithms are iterative for optimum performance, in practice the frequency correction of a single iteration is often adequate, although phase correction generally derives additional benefit from further iterations. Once residual migration effects are contained within a range resolution cell, then conventional iterative autofocus techniques may be employed to "finish" the job.

A block diagram of this technique is given in Figure 6. The process begins with the phase history data. If significant deterministic migration exists, then it will first need to be mitigated with resampling. For relatively coarse resolution images, resampling may not be necessary. The phase history data is then formed into an image with a suitably coarse range resolution. Many conventional autofocus algorithms require some preliminary analysis of a completed (formed) image. The coarse-range-resolution image is then input to a conventional autofocus algorithm such as PGA. The phase error

function is extracted, and the motion error ε_n (or equivalent) is ascertained. Phase and frequency corrections are then applied to the entire phase history data. Image formation is then performed to the resolution that the data allows. Finally, a conventional autofocus algorithm such as PGA may be applied to the full-resolution image to further refine the focus, should the image require this.

Results of this technique are illustrated in Figure 7.

We note that even if only a phase correction (and not the frequency correction) is applied with the error found in this manner, the image often still exhibits a marked improvement over those with only conventional autofocus techniques applied. This is illustrated in Figure 8 where the double-image degradation is corrected, although the trihedral reflectors are not as well focused as in Figure 7.

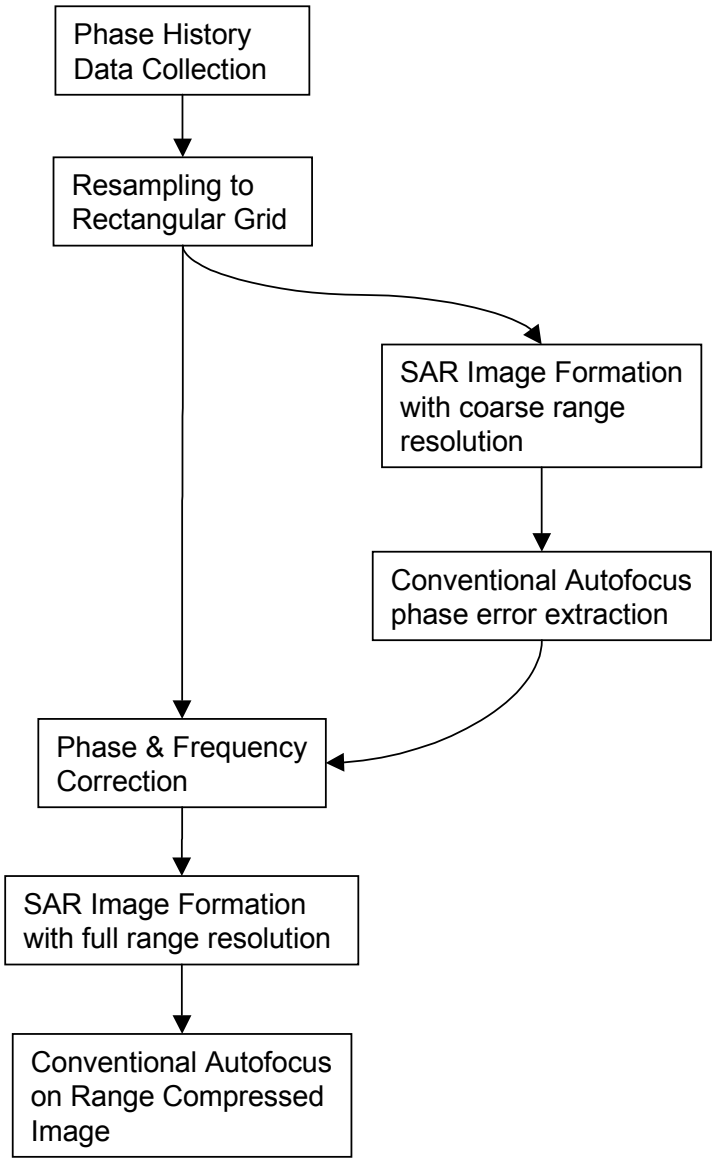

Figure 6. Block diagram detailing processing steps for Technique 1.

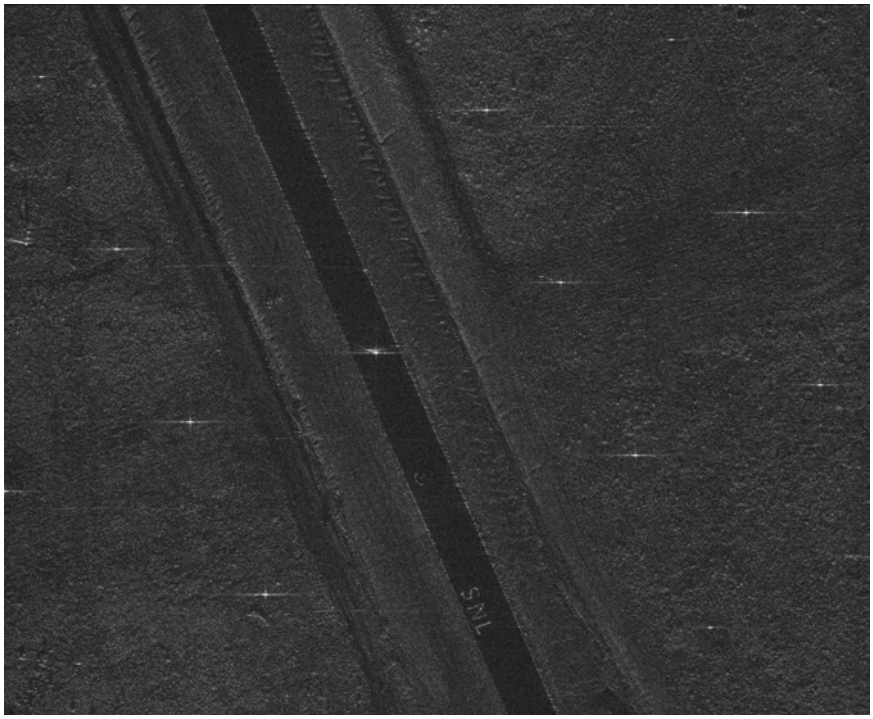

Figure 7. Results of autofocus using technique 1 applied to SAR image.

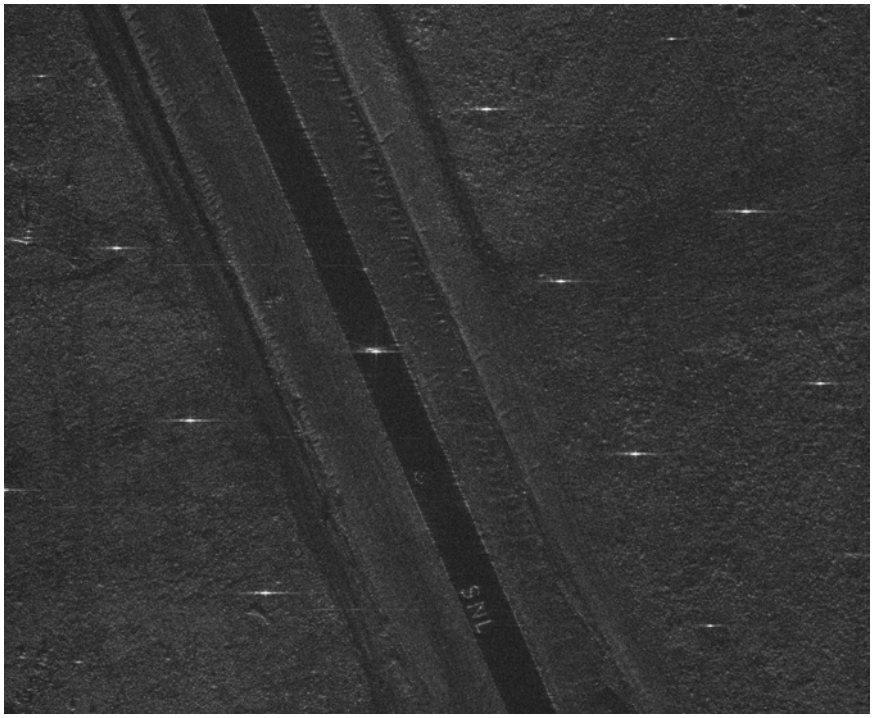

Figure 8. Suboptimal autofocus with only phase correction applied.

While we have discussed finding the quantity ε_n, it should be obvious that any quantity proportional to ε_n would also suffice.

If range subapertures are used for image formation, then perhaps a single range subaperture might be employed for phase-error measurement.

Technique 2:

The essence of this technique is to measure a range shift directly in the range-compressed data, and then compensate the phase history data with phase and frequency corrections.

This technique is reminiscent of the Prominent Point Processing (PPP), but with important and substantial differences. PPP requires selecting a point-like target to "track" in the range-compressed data. This is inadequate for a general purpose autofocus algorithm because prominent point-like targets may not exist in the field of view of the radar. Instead, to overcome the shortcomings of PPP, we propose correlating the entire range profile to establish a shift-gradient in the slow-time dimension.

Note that the range profile of a single point scatterer is given by

$$\text{range profile} \approx \left| A_s \operatorname{csinc}_{I'}\left(\left(\frac{\varepsilon(d\alpha\, n') - \left(\frac{d\varepsilon(\alpha_n)}{d\alpha_n} \right) d\alpha\, n' - s_r}{\rho_r} \right) - v \right) \right|. \tag{31}$$

As the error varies on a pulse-to-pulse basis, so does the peak value position for index v. We define the total apparent shift as

$$\varepsilon_{\text{apparent},n'} \approx \varepsilon(d\alpha\, n') - \left(\frac{d\varepsilon(\alpha_n)}{d\alpha_n} \right) d\alpha\, n'. \tag{32}$$

This is true for all scatterers at all ranges. In fact, as the peak varies on a pulse-to-pulse basis, so does the entire range profile shift proportionately. The nature of SAR data is that adjacent range profiles are very similar in shape, with the shape similarity diminishing with larger separations in index n'.

Comparing the profiles for different pulses n' will reveal a shift in the profiles that can only be dependent on changes in $\varepsilon_{\text{apparent},n'}$. Consequently, by comparing adjacent pulses for the entire data set, a gradient $\Delta\varepsilon_{\text{apparent},n'}$ is determined. By accumulating the gradients $\Delta\varepsilon_{\text{apparent},n'}$, the actual function $\varepsilon_{\text{apparent},n'}$ can be calculated to within an inconsequential constant bias.

In practice, the pulse-to-pulse error gradient $\Delta\varepsilon_{\text{apparent},n'}$ is very small, and difficult to measure accurately. However, several enhancements to the basic procedure alleviate this difficulty.

First, the range profile can be interpolated to a much finer spacing by some factor a_{os} to allow measuring very small shifts in the correlation process. This interpolation can be implemented by zero-padding the pre-range-compressed data set in the fast-time dimension to some new length $a_{os}I'$ prior to the initial range compression, as is well known in the art of digital signal processing.

Second, since the gradient $\Delta\varepsilon_{\text{apparent},n'}$ is in practice a relatively smooth function, it need not necessarily be calculated between adjacent pulses. It is generally sufficient to calculate an approximate gradient over a fairly large number of pulses, under the presumption that if some pulse n' is compared with some other pulse $(n'+n_0)$, then the shift between these pulses is amplified from the pulse-to-pulse gradient by a factor n_0. That is, we presume that

$$\Delta\varepsilon_{\text{apparent},n'} \approx \frac{\varepsilon_{\text{apparent},n'+n_0} - \varepsilon_{\text{apparent},n'}}{n_0}. \tag{32}$$

A rule-of-thumb for selecting n_0 based on minimum slope arguments for a quadratic error might be

$$n_0 \geq N'/\left(2\sqrt{2}a_{os}\right) \tag{33}$$

although values for n_0 even as small as 1/10 the lower limit often work well in practice.

Once a gradient has been ascertained, an accumulation of the gradients yields an approximation of the actual function $\varepsilon_{\text{apparent},n'}$ to within an inconsequential constant bias. The $\varepsilon_{\text{apparent},n'}$ can be averaged to calculate a bias which can then be subtracted. Since $\varepsilon_{\text{apparent},n'}$ is generally a smooth function, the estimate of $\varepsilon_{\text{apparent},n'}$ using this technique can be smoothed to remove discontinuities and other unlikely anomalies resulting from measurements of noisy data.

As before, in practice the frequency correction to the pre-range-compressed data need only be adequate to align the range profiles to within a range resolution cell width. With frequency corrections applied, additional and perhaps more accurate phase corrections can be then calculated using conventional autofocus techniques in the usual manner.

A block diagram of the processing steps for this technique is given in Figure 9. As with the first technique, the process begins with the phase history data. If significant deterministic migration exists, then it will first need to be mitigated with resampling. For relatively coarse resolution images, resampling may not be necessary. The data is then range-compressed with some degree of oversampling. The resulting range profiles are then correlated with some non-adjacent neighbor to enhance sensitivity to shift gradient. The gradients are then accumulated and smoothed to estimate the residual migration. This estimate is then used to correct the phase history data which then undergoes image

formation in the usual manner. Subsequent conventional autofocus algorithms then may be applied to further focus the image.

The results of this technique are illustrated in Figure 10.

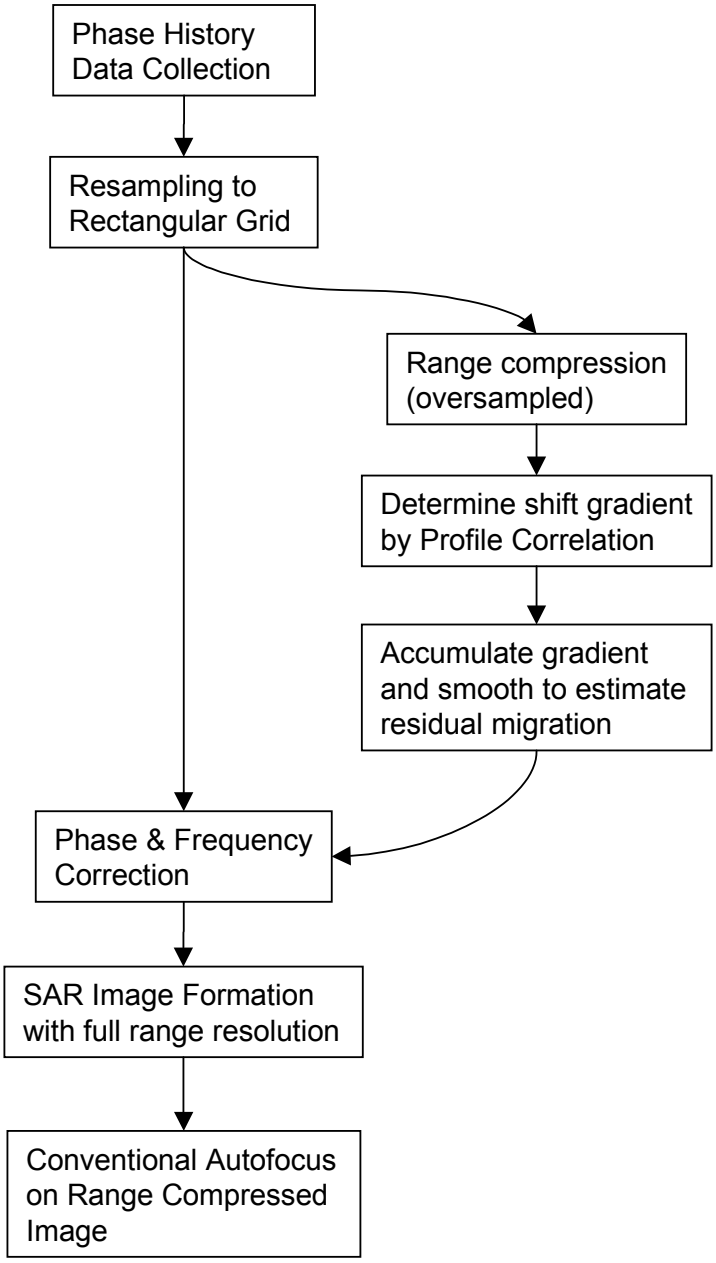

Figure 9. Block diagram illustrating processing steps for technique 2.

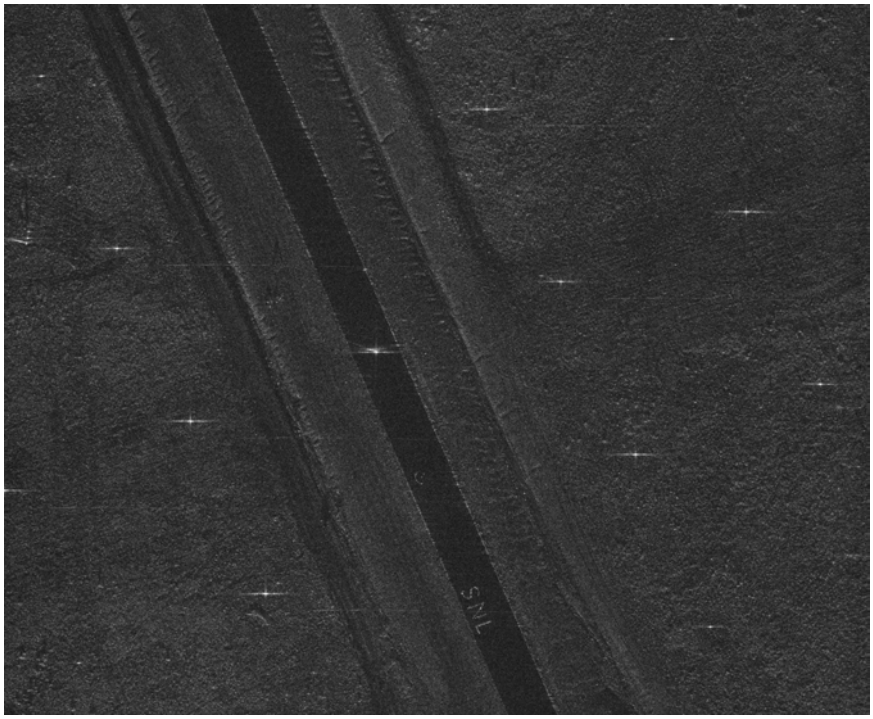

Figure 10. Results of autofocus using technique 2 applied to SAR image.

It should be noted that while the foregoing embodiments of migration correction autofocus begin with phase history data, such data may not be available or convenient. Undoing the azimuth and range compression operations on a complex image provides an equivalent to resampled phase history data that will generally suffice for this purpose. In this manner, even an image that has had conventional autofocus algorithms applied to it may be further corrected by this second technique.

Furthermore, techniques 1 and 2 may be combined and sequentially applied if proper relationships are maintained between error phase and frequency.

4. Conclusions

The following essential elements of this report are summarized.

- Excessive residual migration due to motion errors, or apparent motion errors due in fact to atmospheric propagation phenomena, are not correctable with conventional autofocus algorithms.

- Excessive migration errors require corrections to be applied before final range compression.

- Excessive migration errors require both a frequency correction as well as a phase correction to be applied before final range compression.

- Correcting excessive migration in polar-reformatted data requires correcting for both the motion error and the azimuthal derivative of the motion error.

- Applying only a properly ascertained phase correction might improve the image, but not to the greatest extent possible.

- Excessive migration can be determined by performing conventional autofocus steps on a reduced-range-resolution image, provided the reduced range-resolution is coarser than the residual migration.

- Excessive migration can also be determined by correlating range profiles in range-compressed data.

- Sensitivity to range profile shifts, and hence migration, can be enhanced by oversampling the range compressed data in the range dimension.

- Sensitivity to profile shifts, and hence migration, can also be enhanced by correlating range profiles that are separated in the slow-time dimension.

5. References

[1] J. L. Walker, "Range-Doppler Imaging of Rotating Objects," IEEE Trans. on Aerospace and Electronic Systems, AES-16 (1), 23-52, (1980).

[2] D. E. Wahl, P. H. Eichel, D. C. Ghiglia, C. V. Jakowatz Jr., "Phase Gradient Autofocus – A Robust Tool for High Resolution SAR Phase Correction", IEEE Transactions on Aerospace and Electronic Systems, Vol. 30, No. 3, pp.827-834, July, 1994.

[3] C. V. Jakowatz Jr., D. E. Wahl, P. H. Eichel, D. G. Ghiglia, P. A. Thompson, *Spotlight-Mode Synthetic Aperture Radar: A Signal Processing Approach*, ISBN 0-7923-9677-4, Kluwer academic Publishers, 1996.

[4] W. G. Carrara, R. S. Goodman, R. M. Majewski, *Spotlight Synthetic Aperture Radar Signal Processing Algorithms*, ISBN 0-89006-728-7, Artech House, Inc., 1995.

[5] M. Denny, I. Scott, "Anomalous Propagation Limitations to High-Resolution SAR Performance", Proceedings of the 2002 IEEE Radar Conference, Long Beach, CA, USA, p. 249-254, 22-25 April 2002.

[6] Bryan L. Burns, J. Thomas Cordaro, "Imaging synthetic aperture radar", US Patent 5,608,404, March 4, 1997.

DISTRIBUTION

Unlimited Release

1	MS 0509	M. W. Callahan	2300
1	MS 0529	B. L. Remund	2340
1	MS 0529	B. L. Burns	2340
1	MS 0519	W. H. Hensley	2342
1	MS 0519	S. D. Bensonhaver	2342
1	MS 0519	T. P. Bielek	2342
1	MS 0519	A. W. Doerry	2342
1	MS 0519	D. Harmony	2342
1	MS 0519	J. A. Hollowell	2342
1	MS 0519	S. S. Kawka	2342
1	MS 0519	M. S. Murray	2342
1	MS 0519	B. G. Rush	2342
1	MS 0519	D. G. Thompson	2342
1	MS 0519	L. M. Wells	2344
1	MS 0519	D. L. Bickel	2344
1	MS 0519	J. T. Cordaro	2344
1	MS 0519	J. M. Delaurentis	2344
1	MS 0519	A. Martinez	2344
1	MS 0529	K. W. Sorensen	2345
1	MS 0529	D. F. Dubbert	2345
1	MS 0529	F. E. Heard	2345
1	MS 0529	G. R. Sloan	2345
1	MS 0519	S. M. Becker	2348
1	MS 0519	S. M. Devonshire	2348
1	MS 0519	P. A. Dudley	2348
1	MS 0519	M. W. Holzrichter	2348
1	MS 0519	G. D. Martin	2348
1	MS0519	D. M. Small	2348
1	MS 0519	A. D. Sweet	2348
1	MS 0519	M. E. Thompson	2348
1	MS 0519	B. L. Tise	2348
1	MS 0501	S. M. Kohler	2334
1	MS 0501	M. C. Dowdican	2338
1	MS 0501	T. J. Kim	2338
1	MS 1207	C. V. Jakowatz, Jr.	5937
1	MS 1207	N. E. Doren	5937
1	MS 1207	P. H. Eichel	5937
1	MS 1207	I. A. Erteza	5937
1	MS 1207	D. E. Wahl	5937
1	MS 0328	F. M. Dickey	2612
1	MS 9018	Central Technical Files	8945-1
2	MS 0899	Technical Library	9616
1	MS 0612	Review & Approval Desk for DOE/OSTI	9612
1		Randy Bell	DOE NNSA NA-22
1		Eric Sander	DOE NNSA NA-22